Link to publication

University of Bath

Hydrodynamic Voltammetry at a Rocking Disc Electrode: Theory *versus* Experiment

Sunyhik D. Ahn [a], Karthik Somasundaram [b], H. Viet Nguyen [c], Erik Birgersson [b],
Jim Yang Lee [b], Xiangming Gao [c], Adrian C. Fisher [c], Paul E. Frith [a], and Frank Marken*[a]

[a] *Department of Chemistry, University of Bath, Claverton Down, Bath BA2 7AY, UK*
[b] *Department of Chemical and Biomolecular Engineering, National University of Singapore, Singapore, 117576, Singapore*
[c] *Department of Chemical Engineering, University of Cambridge, New Museums Site, Pembroke Street, Cambridge, CB2 3RA, UK*

Proofs to F. Marken

Email F.Marken@bath.ac.uk

1

Abstract

Rocking disc electrode voltammetry (RoDE) is introduced as an experimentally convenient and versatile alternative to rotating disc voltammetry. A 1.6 mm diameter disc electrode is employed with an overall rocking angle of $\Theta = 90$ degree applied over a frequency range of 0.83 Hz to 25 Hz. For a set of known aqueous redox systems (the oxidation of $Fe(CN)_6^{4-}$ in 1 M KCl, the reduction of $Ru(NH_3)_6^{3+}$ in 0.1 M KCl, the oxidation of hydroquinone in 0.1 M pH 7 phosphate buffer, the oxidation of I^- in 0.125 M H_2SO_4, and the reduction of H^+ in 1 M KCl) the mass transport controlled limiting current I_{lim} is demonstrated to follow in good approximation the Levich-type expression $I_{lim} = 0.111\, nFAcD^{2/3}v^{-1/6}\sqrt{\Theta f}$ with n, the number of electrons transferred per molecule diffusing to the electrode surface, F, the Faraday constant, A, the geometric area, c, the concentration of the active redox species, D, the diffusion coefficient, v, the kinematic viscosity, Θ is the overall rocking angle in degree, and f, the rocking rate in Hz. Quantitative theory is developed based on a two-dimensional (2D) axisymmetric laminar flow model accounting for the conservation of mass, momentum and species along with the kinematic analysis of a "four-bar mechanism" to obtain the rocking motion.

Keywords: Hydrodynamic modulation; Plating; Ionic liquid; Convection; Viscosity.

1. Introduction

Hydrodynamic electrochemical methods, and in particular the rotating disc electrode [1,2,3,4], offer an accurate and reliable way of obtaining surface and solution kinetic information for electrochemical redox systems. Steady state (time independent) voltammetric responses are measured and analysed as a function of the rotation rate. Although more accurate treatments of the hydrodynamic conditions at the rotating disc electrode are known [5], the equation proposed by Levich [6] (see equation 1) is generally accepted for the analysis of the mass transport limited current signals.

$$I_{\text{lim}} = 0.62 \frac{nFAD^{2/3}}{v^{1/6}} \sqrt{2\pi f} = 1.55 \frac{nFAD^{2/3}}{v^{1/6}} \sqrt{f} \tag{1}$$

In this equation, the mass transport limited current I_{lim} is given by n, the number of electrons transferred per molecule diffusing to the electrode surface, F, the Faraday constant, A, the geometric electrode area, D, the diffusion coefficient, v, the kinematic viscosity, and f, the angular frequency given by 2π multiplied by the rotation rate. Many further methods have been developed from the initial concept including, for example, rotating ring-disc measurements [7], high speed turbulent rotating disc voltammetry [8], hydrodynamically modulated rotating disc voltammetry [9], channel flow electrodes [10], and hydrodynamic electrodes with Couette flow [11].

Here, the use of a "rocking" electrode (with overall 90 degree rocking angle, see Figure 1) is contrasted to conventional rotating disc methods. Earlier experimental studies by Cummings *et al.* [12,13] suggested that a "rocking movement" of the electrode (or the electrochemical cell) could lead to uniform mass transport and beneficial electro-deposition conditions very

similar to those obtained with a rotating disc electrode. It was argued that such a system has the advantages of technical simplicity (no sliding contacts) and improved versatility. The study successfully demonstrated that the rocking motion increases the rate of mass transport (the mass transport limited current increased linearly with the square root of the rocking rate) with sufficient electrolyte homogenisation as well as dislodging gas bubbles from the electrode surface. In a further study, the effect of rocking movement on two adjacent semi-disc electrodes was investigated and it was proposed that the angular movement in a given time accounted for the current in a similar manner for rotating disc and for rocking disc systems [14].

In order to further explore the physicochemical characteristics and applications of rocking disc voltammetry (RoDE, see Figure 1), this study systematically investigates the relationship between the mass transport limited current generated by the rocking motion of a 1.6 mm diameter platinum disc electrode. The rocking motion is introduced by linking a rotating plate to a second axis via a "four bar mechanism" (see Figure 1A) with an equivalent mechanism employed in the theory (see Figure 1B). It is shown that in spite of the more complex nature of the hydrodynamic conditions at the rocking disc – solution interface, well-defined voltammetric measurements are possible and a "Levich-type" equation is obtained (in the limit of laminar flow). Future applications of the rocking disc voltammetry method could be in electro-deposition or electro-polishing, etching, electroanalysis, or the voltammetric investigation of complex liquids.

Figure 1

2. Theory

A four-bar mechanism is designed to deliver the rocking motion to the electrode that covers 180 degrees (90 degrees back and forth, see Figure 1B) during one rocking cycle. In practice, the new construction obviates the need for contact brushes and simplifies the experimental procedures. However, the hydrodynamic flow caused by the rocking motion is significantly more complex and no analytical solution is currently available. This problem is thus tackled using a numerical approach. This article aims to numerically investigate the performance of RoDE under a simple electrochemical reaction and to validate it with experimental results. The mathematical model comprises of the governing transient conservation of mass, momentum and species along with the velocity equations for the rocking motion. The nomenclature for symbols is summarised in Table 1 and Table 2.

Table 1. Nomenclature of symbols used in this report.

Symbol	Description
A	disc electrode surface area, m^2
c_i	concentration of species i, mol m^{-3}
c_i^*	bulk concentration of species i, mol m^{-3}
D_i	diffusion coefficient of species i, m^2 s^{-1}
dE/dt	voltage scan rate, V s^{-1}
E_0	initial voltage, V
E_{app}	applied voltage, V
E_{eq}	reference/equilibrium potential, V
F	Faraday's constant, C mol^{-1}
f	body force or inertial force, m s^{-2},
g	acceleration due to gravity, m s^{-2}
h_b	height of beaker, m
h_e	height of electrode holder, m
i_{loc}	charge transfer current density, A m^{-2}
I	current, A
k_a, k_c	anodic and cathodic reaction rate constants, m s^{-1}
N	angular speed, rpm
$\mathbf{N}_i$	flux of species i, mol m^{-2} s^{-1}

n	normal vector, -
n	number of electrons, -
p	pressure, Pa
R	universal gas constant, J mol^{-1} K^{-1}
r	radial coordinate, m
r_b	radius of beaker, m
r_e	radius of disc electrode, m
r_o	radius of electrode holder, m
s_i	stoichiometric coefficient of species I, -
T	temperature, K
t	time, s
u	velocity vector, m s^{-1}
u_r	velocity in r-direction, m s^{-1}
u_θ	velocity in θ-direction, m s^{-1}
u_z	velocity in z-direction, m s^{-1}
z	axial coordinate, m
z_i	charge number, -
θ	angular coordinate, rad
Θ	total rocking angle, degree
Greek	
α	transfer coefficient, -
η	overpotential, V
μ	dynamic viscosity of the electrolyte, Pa s
ν	kinematic viscosity of the electrolyte, m^2 s^{-1}
ρ	density of the electrolyte, kg m^{-3}
ϕ_l	potential in the electrolyte, V
ω	angular velocity of the rotating electrode, rad s^{-1}
Subscript	
i	Species (O - oxidizing, and R – reducing species)

Table 2. Physical parameters.

Parameter	Value
c_O^0	0 mol m^{-3}
c_R^0	1 mol m^{-3}
$\dfrac{dE}{dt}$	0.01 V s^{-1}
D_i	0.65 x 10^{-9} m^2 s^{-1}
E_0	-0.1 V
E_{eq}	0.21 V
F	96487 C mol^{-1}
h_b	2 x 10^{-2}m
h_e	1 x 10^{-2} m
k_a , k_c	8 x 10^{-5} m s^{-1}
n	1

r_b	3 x 10^{-2} m
r_e	8 x 10^{-4} m
r_o	4 x 10^{-3} m
R	8.314 J mol-1 K^{-1}
s_R	-1
s_O	1
T	298.15 K
$\mathcal{E}$	0.5
μ	10^{-3} Pa s
ρ	10^3 kg m^{-3}
ϕ_l	0 V

Kinematic analysis of the four-bar mechanism yields the velocity equations that are solved numerically to obtain the rocking rate in terms of the rotation rate (see Figure 1D). The rocking motion obtained is fed as the boundary condition to the transient conservation of momentum and thus gets coupled. The limiting current corresponding to various "rocking" frequencies will be calculated and compared to both experimental data and the theoretical values from a modified Levich-type equation.

A key difference between the classic rotating disc electrode (RDE) and the rocking disc electrode (RoDE) is the introduction of a "rocking" mechanism. A schematic of the whole device and the mechanism is illustrated in Figure 1A. The four-bar mechanism (Figure 1B) functions as follows. The bar AB is rotated at regular frequency "ω_2", which can be electronically controlled with a motor. Via the crank BC, this transmits a "back-and-forth" motion to the bar CD. The electrode is attached to the bar CD and its movement then follows that of the bar. The "rocking" frequency used in subsequent parts of the article will refer to the frequency of bar AB instead of CD. By denoting the angles θ_2, θ_3 and θ_4 as in Figure 1B, the

following differential equations termed as velocity equations are obtained from kinematic analysis:

$$\frac{d\theta_3}{dt} = \frac{L_2}{L_3}\omega_2\frac{\sin(\theta_2 - \theta_4)}{\sin(\theta_4 - \theta_3)} \tag{1}$$

$$\frac{d\theta_4}{dt} = \frac{L_2}{L_4}\omega_2\frac{\sin(\theta_2 - \theta_3)}{\sin(\theta_4 - \theta_3)} \tag{2}$$

Here ω_2 is the angular frequency of bar AB in rad/s, L_2, L_3, and L_4 are the lengths of the links as shown in Figure 1B. The equations above are subject to appropriate initial conditions for θ_3 and θ_4 from the geometry of the mechanism. The rocking rate is given by Eq. 2 and the Levich equation now will have additional terms other than ω_2. Once the rocking rate $\frac{d\theta_4}{dt}$ is calculated, it is coupled to the fluid and mass transport calculations as outlined below.

Fluid and species transport. A schematic representation of the RoDE experimental setup is shown in Figure 1C. The disc electrode is immersed in a large beaker containing an aqueous solution of the electrolyte using an electrode holder made of Teflon. Excess supporting electrolyte is used and a generalised redox process O + e⁻ ⇌ R is considered. The continuity equation for incompressible fluids is given by equation 3.

$$\nabla \cdot \mathbf{u} = 0 \tag{3}$$

The momentum conservation for the fluid is given by equation 4.

$$\frac{\partial \mathbf{u}}{\partial t} + \mathbf{u} \cdot \nabla\mathbf{u} = -\frac{1}{\rho}\nabla p + v\,\nabla^2\mathbf{u} + f \tag{4}$$

The species conservation equation is described by equation 5.

$$\frac{\partial c_i}{\partial t} = -\nabla \cdot \mathbf{N}_i + r_i, i = 0, R \tag{5}$$

The flux here is defined in equation 6.

$$\mathbf{N}_i = -D_i \nabla c_i - z_i u_i F c_i \nabla \phi_l + \mathbf{u} c_i, \tag{6}$$

In the above equations, $\mathbf{u}$ is the velocity vector, t is the time, p is the pressure, ρ is the density of the electrolyte, ν is the kinematic viscosity of the electrolyte, c_i is the concentration of the species i, $\mathbf{N}_i$ is the species flux, r_i is the rate of homogenous production of species i, D_i is the diffusion coefficient of species i, z_i is the charge number, u_i is the species mobility, F is the Faraday's constant, and ϕ_l is the potential in the electrolyte. In equation 6, the first term on the right hand side denotes the diffusive flux, the second term represents the flux due to migration, and the third term provides the convective flux. For solutions containing an excess of supporting electrolyte, the ionic migration term can be neglected and hence the second term becomes zero. The liquid phase potential is also set to zero. Without chemical reactions in solution and diffusion coefficients assumed constant, the general convective-diffusion (equation 7) is obtained.

$$\frac{\partial c_i}{\partial t} = D_i \nabla^2 c_i - \mathbf{u} \cdot \nabla c_i \tag{7}$$

For the case of a liquid with a constant density and a constant binary diffusion coefficient, continuity, and the geometry as shown in Figure 1C, momentum and species balance equations are transformed into cylindrical coordinates as shown in equations 8-12 below.

Continuity

$$\frac{1}{r} \frac{\partial}{\partial r} (r u_r) + \frac{1}{r} \frac{\partial u_\theta}{\partial \theta} + \frac{\partial u_z}{\partial z} = 0 \tag{8}$$

Momentum conservation (r - component)

9

$$\rho \frac{\partial u_r}{\partial t} + \rho u_r \frac{\partial u_r}{\partial r} + \rho \frac{u_\theta}{r} \frac{\partial u_r}{\partial \theta} - \rho \frac{u_\theta^2}{r} + \rho u_z \frac{\partial u_r}{\partial z} =$$

$$-\frac{\partial p}{\partial r} + \mu \frac{\partial}{\partial r}\left[\frac{1}{r}\frac{\partial}{\partial r}(ru_r)\right] + \frac{\mu}{r^2}\frac{\partial^2 u_r}{\partial \theta^2} - \mu \frac{2}{r^2}\frac{\partial u_\theta}{\partial \theta} + \mu \frac{\partial^2 u_r}{\partial z^2} \tag{9}$$

Momentum conservation (θ-component)

$$\rho \frac{\partial u_\theta}{\partial t} + \rho u_r \frac{\partial u_\theta}{\partial r} + \rho \frac{u_\theta}{r} \frac{\partial u_\theta}{\partial \theta} + \rho \frac{u_r u_\theta}{r} + \rho u_z \frac{\partial u_\theta}{\partial z} =$$

$$-\frac{1}{r}\frac{\partial p}{\partial \theta} + \mu \frac{\partial}{\partial r}\left[\frac{1}{r}\frac{\partial}{\partial r}(ru_\theta)\right] + \frac{\mu}{r^2}\frac{\partial^2 u_\theta}{\partial \theta^2} + \mu \frac{2}{r^2}\frac{\partial u_r}{\partial \theta} + \mu \frac{\partial^2 u_\theta}{\partial z^2} \tag{10}$$

Momentum conservation (z -component)

$$\rho \frac{\partial u_z}{\partial t} + \rho u_r \frac{\partial u_z}{\partial r} + \rho \frac{u_\theta}{r} \frac{\partial u_z}{\partial \theta} + \rho u_z \frac{\partial u_z}{\partial z} = -\frac{\partial p}{\partial z}$$

$$+\frac{\mu}{r}\frac{\partial}{\partial r}\left[r\frac{\partial u_z}{\partial r}\right] + \frac{\mu}{r^2}\frac{\partial^2 u_z}{\partial \theta^2} + \mu \frac{\partial^2 u_z}{\partial z^2} \tag{11}$$

Species conservation

$$\frac{\partial c_i}{\partial t} + u_r \frac{\partial c_i}{\partial r} + \frac{u_\theta}{r}\frac{\partial c_i}{\partial \theta} + u_z \frac{\partial c_i}{\partial z} = D_i \left[\frac{1}{r}\frac{\partial}{\partial r}\left(r\frac{\partial c_i}{\partial r}\right) + \frac{1}{r^2}\frac{\partial^2 c_i}{\partial \theta^2} + \frac{\partial^2 c_i}{\partial z^2}\right] \tag{12}$$

In the above equations 8-12, u_r is the radial component of velocity, u_θ is the angular component of the velocity, u_z is the axial component of the velocity, μ is the dynamic viscosity of the fluid, r is the radial coordinate, θ is the angular coordinate, and z is the axial coordinate.

Boundary and initial conditions. At the walls of the beaker ($r = r_b, -h_e \le z \le h_b - h_e$, and $z = h_b - h_e, 0 \le r \le r_b$), no slip is specified for the velocity and no flux is specified for the species (equation 13).

$$u_r = u_\theta = u_z = 0, \mathbf{n} \cdot \mathbf{N}_i = 0 \tag{13}$$

At the surface of the disc electrode ($z = 0, 0 \le r \le r_e$), redox reactions provide the flux of the

oxidized and reduced species (equation 14).

$$\mathbf{n} \cdot \mathbf{N}_i = \frac{s_i i_{loc}}{F} \tag{14}$$

As the disc electrode along with the holder spins at the specified revolutions per minute (rpm), the velocity is specified at these boundaries ($z = 0, 0 \le r \le r_o$ and $r = r_o, -h_e \le z \le 0$) as in equation 15.

$$u_r = u_z = 0 \tag{15}$$
$$u_\theta = \frac{d\theta_4}{dt} r$$

Insulation is specified at the electrode holder boundary as no species flow across the holder occurs ($z = 0, r_e \le r \le r_o$ and $r = r_o, -h_e \le z \le 0$, equation 16).

$$\mathbf{n} \cdot \mathbf{N}_i = 0 \tag{16}$$

At the top free/open surface of the electrolyte ($z = -h_e, r_o \le r \le r_b$), symmetry boundary conditions are applied for fluid flow and species transport which denotes that there is no normal stress on the fluid here and no flux of species (equation 17).

$$\frac{\partial u_r}{\partial z} = \frac{\partial u_\theta}{\partial z} = u_z = 0 \tag{17}$$
$$\mathbf{n} \cdot \mathbf{N}_i = 0$$

For the 2D axisymmetric case, axial symmetry is specified at the axis of cylindrical coordinate ($r = 0$, equation 18).

$$u_r = u_\theta = \frac{\partial u_z}{\partial r} = 0 \tag{18}$$

The pressure is set to be zero arbitrarily at a reference point ($r_0 < r = r_b, z = -h_e$).

$$p = 0 \tag{19}$$

At time $t = 0$, the concentration of reduced and oxidised species are defined in equation 20.

$$c_i = \begin{cases} c_R^0, i = R \text{ (reduced species)} \\ c_O^0, i = O \text{ (oxidizing species)} \end{cases} \qquad (20)$$

Constitutive relations. The transfer current density is defined by using Butler-Volmer kinetics (equation 21).

$$i_{loc} = nF\left(k_a c_R \, \exp\left(\frac{(1-\beta)\eta F}{RT}\right) - k_c c_O \, \exp\left(\frac{-\beta\eta F}{RT}\right)\right), \qquad (21)$$

Here the overpotential η is defined as

$$\eta = E_{app} - \phi_l - E_{eq}. \qquad (22)$$

The voltage applied at the electrode depends on the scan rate and is defined as

$$E_{app} = E_0 + \frac{dE}{dt}t \qquad (23)$$

The current is the flux at the electrode surface and is defined as

$$I = \pm nFAD_i\left(\frac{dc_i}{dy}\right)_{y=0}, i = O, R \qquad (24)$$

with + sign used for the oxidized species and – sign for the reduced species respectively. The expression for the Levich equation (equation 25) for a RDE is

$$i_{Levich,RDE} = 0.62 \, nFAc^* D^{\frac{2}{3}} v^{-\frac{1}{6}} \sqrt{\omega_2} \qquad (25)$$

where $c^* = \lim_{z\to\infty} c$ represents the bulk concentration of the oxidized or reduced species for cathodic or anodic limiting currents. For a RoDE, we employ the rocking rate instead of the rotational rate to obtain equation 26.

$$i_{Levich,RoDE} = 0.62 \, nFAc^* D^{\frac{2}{3}} v^{-\frac{1}{6}} \sqrt{\frac{d\theta_4}{dt}} \qquad (26)$$

The time average of the absolute values in the sine term in equation 2 along with the given length ratio L_2/L_4 relate the rocking rate to the rotation rate (equation 27). The factor 0.46 (for a total rocking angle 90 degree) is close to $L_2/L_4 = 7$ mm / 10 mm = 0.7, but can be obtained more accurately numerically from the Comsol model by averaging over time. More generally, the rocking rate can be expressed as in equation 27.

$$\frac{d\theta_4}{dt} = 0.46\,\omega_2 \tag{27}$$

Therefore, the Levich-type equation for RoDE (equation 28) can be expressed directly (assuming laminar conditions prevail at the electrode surface – solution interface). Furthermore, the effect of the total rocking angle Θ can be predicted with the model and expressed as shown in the Levich-type expression in equation 29. The corresponding diffusion layer thickness is given in equation 30.

$$i_{Levich,RoDE} = 0.62\,nFAc^*D^{\frac{2}{3}}v^{-\frac{1}{6}}\sqrt{0.46\omega_2} = 1.05\,nFAc^*D^{\frac{2}{3}}v^{-\frac{1}{6}}\sqrt{f} \tag{28}$$

$$i_{Levich,RoDE} = 0.111\,nFAc^*D^{\frac{2}{3}}v^{-\frac{1}{6}}\sqrt{\Theta f} \tag{29}$$

$$\delta_{RoDE} = \frac{9.0D^{\frac{1}{3}}v^{\frac{1}{6}}}{\sqrt{\Theta f}} \tag{3}$$

Numerics. The 2D axisymmetric model equations are solved using the commercial finite element solver Comsol Multiphysics 5.1. The system of equations for the rocking mechanism model is implemented using global ODEs in Comsol and solved with a convergence tolerance

of 10^{-6}. For fluid flow and species transport, the single phase laminar flow and transport of diluted species modes in Comsol are used. The mesh consists of 7×10^3 and 3.3×10^3 elements for the fluid flow and species transport respectively and the corresponding degrees of freedom (DoF) are 50×10^3 and 7.5×10^3. The solutions were tested for mesh independence. Initially, the rocking motion is solved followed by the fluid flow and species transport in sequence. The computations were carried out in a workstation having two quad-core processors with 64GB RAM.

Simulation results. The case of a redox system with $D = 0.65 \times 10^{-9}$ m^{2}s^{-1} and $c = 1$ mM is considered with a 1.6 mm diameter disc electrode giving an area of A $= 2 \times 10^{-6}$ m^2. The voltammograms obtained at various rocking rates (here in rpm) agree well with experimental observations at lower rocking rates as shown in Figure 2. As expected, the limiting current increases with increasing frequency.

Figure 2.

3. Experimental Details

3.1. Chemical Reagents

Potassium chloride (99%), sodium perchlorate (98%), potassium iodide (99%), sulphuric acid (95-98%), and sucrose (99.5%) were obtained from Sigma Aldrich. Hydrochloric acid (30%)

was obtained from Fluka, and hexa-ammine ruthenium (III) chloride (99%) from purchased Strem Chemicals. Reagents were used without further purification. Solutions were prepared in demineralized and filtered water taken from a Thermo Scientific water purification system (Barnstead Nanopure) with 18.2 MΩcm resistivity.

3.2. Instrumentation

For voltammetry studies, a microAutolab II potentiostat system (EcoChemie, Netherlands) was employed with a KCl-saturated calomel reference electrode (SCE, Radiometer). For all experiments, the reference electrode was placed in approximately 2 mm distance from the working electrode. The working electrode was a platinum macrodisc electrode with a diameter of 1.6 mm (BAS). The counter electrode was a platinum wire. Rocking motion (total angle 90 degrees) of the working electrode (as shown in Figure 1) was applied with an IKA Eurostar digital motor. Diffusion coefficients for electrolyte solutions with sucrose-controlled viscosity were determined at a 100 μm diameter platinum microelectrode employing chronoamperometry. Experimental transient data were fitted with DigiElch 4.F software (employing 2D semi-infinite diffusion) to give diffusion coefficients for $Fe(CN)_6^{4-}$ in 1 M KCl as a function of sucrose content. All experiments were conducted in ambient atmosphere at a temperature of 22 +/- 2 °C.

4. Results and Discussion

4.1. Rocking Disc Electrode Voltammetry I.: Convective Transport and Concentration Effects

Initial experiments were performed for the one-electron oxidation of 1 mM $Fe(CN)_6^{4-}$ to $Fe(CN)_6^{3-}$ in aqueous 1 M KCl. For an electrode that is gently rocking at 1.67 Hz (see Figure 2A), the effect of scan rate on the shape of the voltammetric response is indicative of the hydrodynamic effect. Only at a lower scan rate of 10 mVs^{-1} is the peak response insignificant and a near-steady state voltammogram is obtained. The average diffusion layer thickness under these conditions can be estimated based on the scan rate v_{trans} that describes the transition from a transient to the steady state case (see equation 31).

$$\delta \approx \sqrt{\frac{DRT}{v_{trans}F}} = \sqrt{\frac{0.65 \times 10^{-9} \times 8.31 \times 293}{0.01 \times 96487}} = 41\,\mu m \tag{31}$$

In this expression D is the diffusion coefficient for $Fe(CN)_6^{4-}$ (0.65×10^{-9} m^{2}s^{-1} [15]), R is the gas constant, T is the absolute temperature, and F is the Faraday constant. An average diffusion layer thickness of ca. 41 μm is estimated for a rocking rate of 1.67 Hz. This estimate can be compared with the more accurate diffusion layer thickness calculated under these conditions based on equation 30, δ_{RoDE} = 64 μm. By increasing the rocking rate, the limiting current is increased and therefore the average diffusion layer thickness decreased (see Figure 3B). When plotted, the square root dependency of the mass transport limited current on the rocking rate is clearly revealed (see Figure 3C). As expected, the transition scan rate v_{trans} is significantly increased at higher rocking rates.

Figure 3.

The effect of varying concentration of $Fe(CN)_6^{4-}$ on the mass transport controlled limiting current is demonstrated in Figure 4. A plot of the limiting current as a function of concentration is shown for three different rocking rates. The plots demonstrate good linearity in agreement with equation 29.

4.2. Rocking Disc Electrode Voltammetry II.: Effect of Diffusion Coefficient and Viscosity

The effect of the diffusion coefficient on the RoDE limiting current was studied by working with five different redox systems (see Figure 4C): (i) the reduction of 1 mM H^+ in 1 M KCl with a diffusion coefficient of 7.22×10^{-9} m^2s^{-1} [15] (see Figure SI1), (ii) the oxidation of 1 mM I^- in 0.125 M H_2SO_4 with a diffusion coefficient of 1.99×10^{-9} m^2s^{-1} [15] (see Figure SI2), (iii) the reduction of 1 mM $Ru(NH_3)_6^{3+}$ in 0.1 M KCl with a diffusion coefficient of 0.91×10^{-9} m^2s^{-1} [16] (see Figure SI3), (iv) the oxidation of 1 mM hydroquinone in 0.1 M phosphate buffer pH 7 with a diffusion coefficient of 0.75×10^{-9} m^2s^{-1} [15] (see Figure SI4), and (v) the oxidation of 1 mM $Fe(CN)_6^{4-}$ in 1 M KCl with a diffusion coefficient of 0.65×10^{-9} m^2s^{-1} [15]. The double logarithmic plot of the mass transport limited current (divided by the number of transferred electrons) versus D shows a trend in good agreement with the expected $D^{2/3}$ dependence as predicted in equation 29 (Figure 4C).

Figure 4.

The effect of changing viscosity on current responses is more subtle and this is studied here by the addition of sucrose into the aqueous electrolyte solution. Sucrose was electrochemically inert within the potential range of the experiment (using oxidation of 1 mM $Fe(CN)_6^{4-}$ in 1 M KCl) and could be used to adjust the viscosity over a sufficiently large range (see Figure 5A). The change in viscosity of the liquid electrolyte is known to affect the diffusion coefficient of the electroactive species. The diffusion coefficient of $Fe(CN)_6^{4-}$ in 1 M KCl at different sucrose concentrations was determined by microelectrode chronoamperometry at a disc (100 μm diameter, see experimental) and fitting with the simulation software package DigiElch 4.F (employing 2D semi-infinite diffusion) to give reliable diffusion coefficient data (see Figure 5B). To elucidate the effect of the kinematic viscosity on the limiting current a normalisation has to be applied. The double logarithmic plot of the limiting current under rocking disc conditions divided by $D^{2/3}$ *versus* kinematic viscosity (controlled with sucrose [17]) is shown in Figure 5C (see also Figure SI5). The dashed line shows the expected behaviour for $I_{\text{lim}} \propto v^{-1/6}$ within the error of the experimental data. All data are in agreement with equation 29.

Figure 5.

18

5. Conclusions

It has been shown that for rocking frequencies up to 25 Hz for a 1.6 mm diameter inlaid platinum disc, well-defined voltammetry is possible under rocking disc voltammetry conditions. A quantitative expression, $I_{Levich,RoDE} = 0.111\,nFAD^{\frac{2}{3}}v^{-\frac{1}{6}}\sqrt{\Theta f}$, has been introduced based on a model and confirmed by comparison with experimental data. Intriguingly, when selecting the total rocking angle $\Theta = 180$ degree (consistent with a full cycle for RoDE compared to RDE) the equation reverts back into the original Levich equation (with only 3% deviation) indicative of the fact that the angular movement in a given time (and therefore the transferred momentum) accounts for the current in a similar manner for rotating disc and for rocking disc systems.

For the rotating disc electrode (RDE) the laminar flow regime is important and the classical Levich equation only holds for unbounded smooth conditions in fully developed laminar flow. Similarly, for the RoDE system "quasi laminar flow" appears to be important and a transition to turbulent conditions is likely at higher rocking rates. For example, for wall-jet hydrodynamic electrodes [18] the transition to turbulent flow has been expressed in terms of the critical Reynolds number with $25 < Re_{critical} < 1000$ (with $Re = \frac{Ul}{v}$ where U is the velocity in ms^{-1}, l is the nozzle diameter in m, and v is the kinematic viscosity in m^{2}s^{-1}). Similarly, for the rotating disc electrode under high speed conditions [19] the transition to turbulent conditions is expected at $Re_{critical} = 3 \times 10^5$ [20,21] (with $Re = \frac{wr^2}{v}$ where w is the rotation speed in s^{-1}, r is the radius in m, and v is the kinematic viscosity in m^{2}s^{-1}). Due to the higher amount of energy dissipated into the solution during rocking agitation, the corresponding RoDE transition to turbulence is likely to occur at lower frequencies when compared to the transition to turbulent rotating disc conditions. For the preliminary device design reported here additional parameters such as depth

of immersion and size of container may also affect the flux of material to and from the electrode surface. Further experimental work will be required to establish additional parameters and the transition to turbulent conditions. The question whether surface roughness, container shape or symmetry, distance to the container bottom, or gravity can affect the conditions at the RoDE will have to be addressed in future experiments.

Generally, it is possible to summarise the potential pros and cons for RoDE experiments as (i) the RoDE system can be operated without electrical brush contacts, (ii) the rocking agitation is likely to effectively dislodge gas bubbles or particles, (iii) an approximately uniform diffusion layer allows (similar to RDE) plating of metals or thin films evenly over substrates [12,13], (iv) all methods for kinetic analysis of heterogeneous or homogeneous electrode reactions can be applied in a similar way for RoDE and RDE, and (v) electro-synthetic reactions are possible under defined diffusion layer thickness conditions. Possible problems arise from currently unknown effects of the container size and shape with significant changes in flow pattern expected for both RDE and RoDE if there is only a small gap between the container wall and the electrode [22]. For the case of non-Newtonian fluids interesting differences in RDE and in RoDE experiments should emerge. The miniaturisation of the RoDE experiment similar to that for the RDE [23] appears possible and potentially useful.

Future applications of the rocking disc voltammetry methodology are possible in plating or electro-polishing applications, where uniform mass transport and removal of bubbles from electrode surfaces are desirable. Due to the uniform accessibility of the electrode surface, the expression for the limiting current is readily adapted to apply to other electrode shapes (non-circular) and sizes. The interaction of colloid- and micro-particles with the flow field in RDE experiments has been recognised to significantly affect mass transport [24]. This effect can be

predicted to change under RoDE conditions possibly leading to a better interaction of the particles with the electrode surface.

Acknowledgements

References

[1]   W.J. Albery, M.L. Hitchman, Ring-disc electrodes, Clarendon Press, Oxford, 1971.

[2]   A.J. Bard, L.R. Faulkner, Electrochemical methods, fundamentals and applications, 2nd ed., Wiley-Interscience, New York, 2001.

[3]   A.C. Riddiford, The rotating disc system, P. Delahay (ed.), Adv. Electrochem. Electrochem. Eng. 4 (1966) 47-116.

[4]   D. Pletcher, Application of electrochemical techniques to homogeneous chemical reactions, Chem. Soc. Rev. 4 (1975) 471-495.

[5]   J. Newman, Schmidt number correction for rotating disk, J. Phys. Chem. US 70 (1966) 1327-1328.

[6]   V.G. Levich, Physiochemical hydrodynamics, Prentice Hall Inc., Englewood Cliffs, New York, 1962.

[7]   B. Miller, S. Bruckenstein, Hydrodynamic potentiometry and amperometry at ring-disk electrodes, J. Electrochem. Soc. 117 (1970) 1032-1033.

[8]   M. Varadi, M. Gratzl, E. Pungor, Turbulent hydrodynamic voltammetry .2. investigations of turbulence frequency in a hydrodynamic voltammetric cell, Anal. Chim. Acta 83 (1976) 1-8.

[9]   K. Tokuda, S. Bruckenstein, B. Miller, Frequency-response of limiting currents to sinusoidal speed modulation at rotating-disk electrodes, J. Electrochem. Soc. 122 (1975) C110-C110.

[10]   J.A. Cooper, R.G. Compton, Channel electrodes - A review, Electroanalysis, 10 (1998) 141-155.

[11]   C.E. Hotchen, H.V. Nguyen, A.C. Fisher, P.E. Frith, F. Marken, Hydrodynamic microgap voltammetry under couette flow conditions: electrochemistry at a rotating drum in viscous poly(ethylene glycol), ChemPhysChem 16 (2015) 2789-2796.

[12]   C.Y. Cummings, P.E. Frith, G. Zoppi, I. Forbes, K.D. Rogers, D.W. Lane, F. Marken, Rocking disc electro-deposition of copper films on $Mo/MoSe_2$ substrates, Thin Solid Films, 519 (2011) 7458-7463.

[13]   C.Y. Cummings, G. Zoppi, I. Forbes, D. Colombara, L.M. Peter, F. Marken, Rocking disc electro-deposition of CuIn alloys, selenisation, and pinhole effect minimisation in CISe solar absorber layers, Electrochim. Acta 79 (2012) 141-147.

[14]   S.D. Ahn, P.E. Frith, A.C. Fisher, A.M. Bond, F. Marken, Mass transport and modulation effects in rocking dual-semi-disc electrode voltammetry, J. Electroanal. Chem. 722 (2014) 78-82.

[15]   R.N. Adams, Electrochemistry at solid electrodes, Marcel Dekker, New York, 1969, p. 219.

[16]   F. Marken, R.P. Akkermans, R.G. Compton, Voltammetry in the presence of ultrasound: The limit of acoustic streaming induced diffusion layer thinning and the effect of solvent viscosity, J. Electroanal. Chem. 415 (1996) 55-63.

[17]   S. Cha, S.H. Kim, D. Kim, Viscosity of sucrose aqueous solutions measured by using fluorescence correlation spectroscopy, J. Korean Phys. Soc. 56 (2010) 1315-1318.

[18]   H. Gunasingham, B. Fleet, Wall-jet electrode in continuous monitoring voltammetry, Anal. Chem. 55 (1983) 1409–1414.

[19]   C.E. Banks, A.O. Simm, R. Bowler, K. Dawes, R.G. Compton, Hydrodynamic electrochemistry: design for a high-speed rotating disk electrode, Anal. Chem. 77 (2005) 1928–1930.

[20]   O.T. Hanna, O.C. Sandall, G. Ruiz-Ibanez, Turbulent mass-transfer on a rotating-disk, Chem. Eng. Sci. 43 (1988) 1407-1410.

[21]   C. Deslouis, B. Tribollet, L. Viet, Local and overall mass-transfer rates to a rotating-disk in turbulent and transition flows, Electrochim. Acta 25 (1980) 1027-1032.

[22]   V.M. Chiu, P.A. Lukus, J.L. Doyle, J.O. Schenk Mass transport at rotating disk electrodes: effects of synthetic particles and nerve endings, Anal. Biochem. 418 (2011) 58–65.

[23]   X.P. Gao, H.S. White, Rotating Microdisk Voltammetry, Anal. Chem. 67 (1995) 4057-4064.

[24]   R.G. Compton, C.A. Brown, Monitoring particle sizes with rotating-disc electrodes – measurement of the dissolution kinetics of calcite, *J. Coll. Interface Sci.* 158 (1993) 243-246.
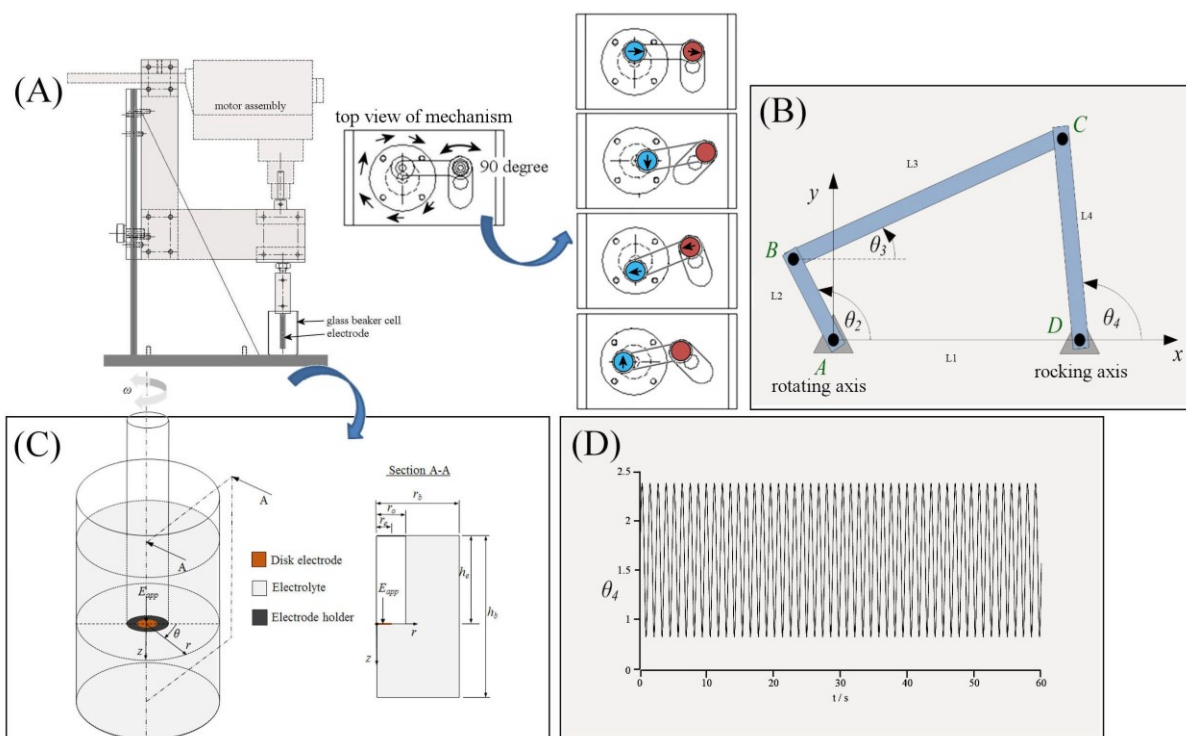
Figure 1. (A) Schematic drawing of the motor driven rocking disc electrode system with cell and electrode assembly. (B) Comsol mechanism for converting rotation into rocking motion. (C) Schematic of the rocking system in 3D and 2D axi-symmetric geometries. (D) Rocking motion as defined by the kinematic analysis (at 50 rpm) described by angular parameter θ_4.
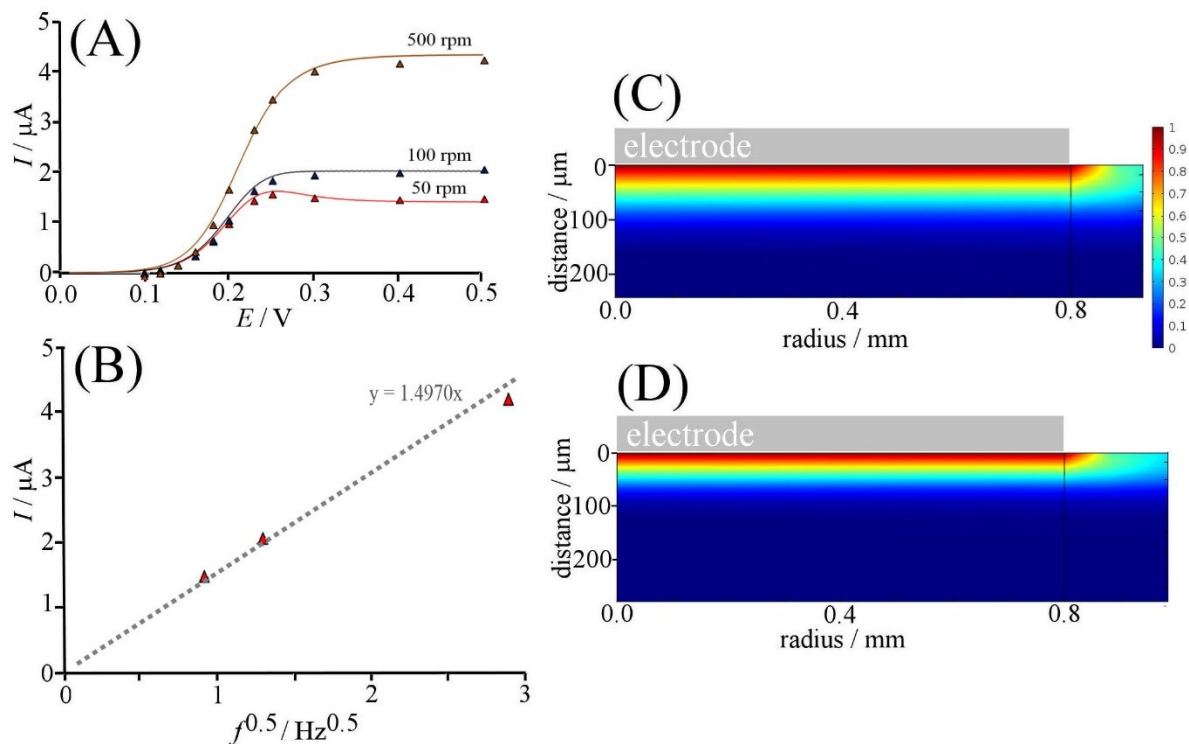
Figure 2. (A) Voltammograms (scan rate 10 mVs^{-1}, 1 mM redox active species, $D = 0.65 \times 10^{-9}$ m^{2}s^{-1}, 1.6 mm diameter disc electrode) at various rocking rates: model predictions (lines) versus experimental data (symbols, *vide infra*). (B) Plot of limiting current versus rocking frequency: model predictions (lines) versus experiments (symbols, *vide infra*). (C,D) Contour maps of the diffusion layer showing the concentration of product at the end of the potential sweep at 0.5 V for (C) 50 rpm and (D) 100 rpm.
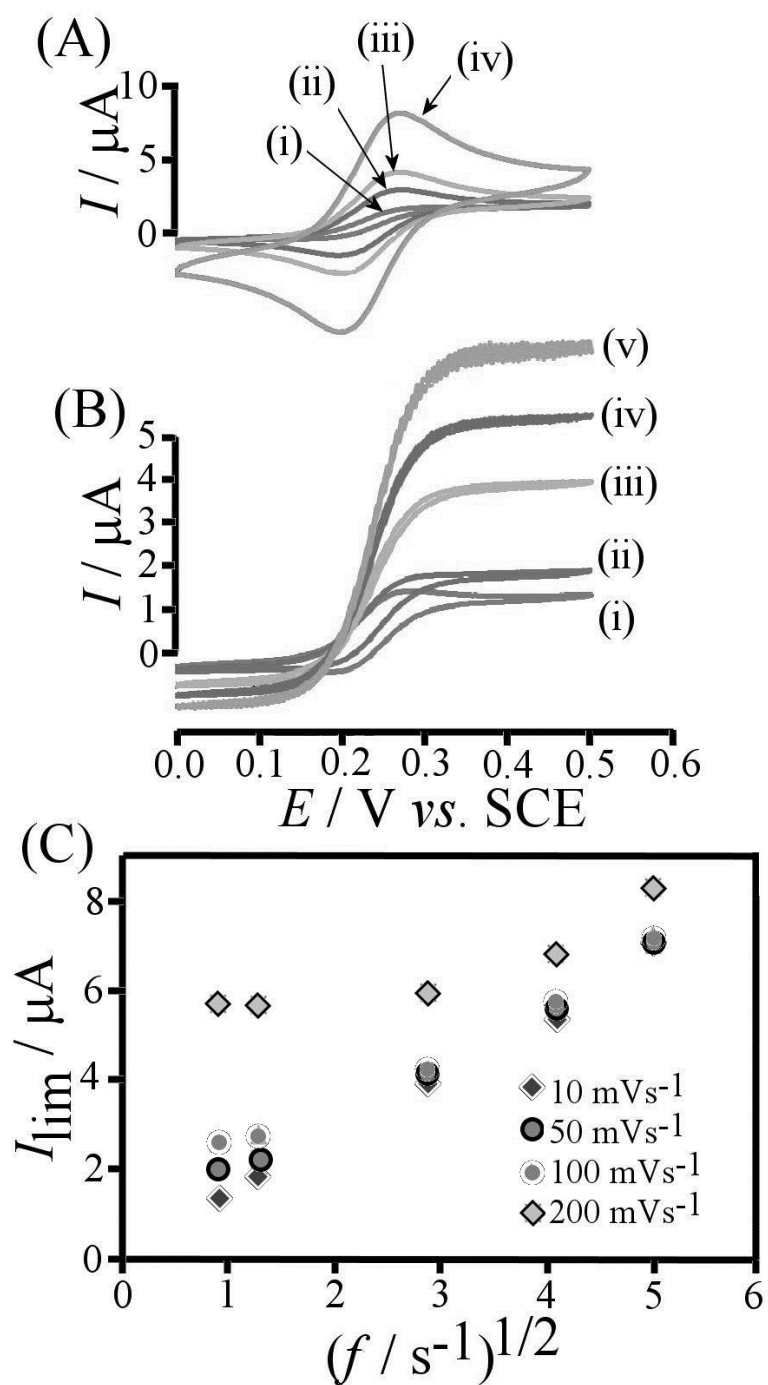
Figure 3. (A) Cyclic voltammograms (scan rate (i) 10, (ii) 50, (iii) 100, and (iv) 400 mVs^{-1}) for the oxidation of 1 mM Fe(CN)$_6^{4-}$ in aqueous 1 M KCl at a rocking (1.67 Hz) 1.6 mm diameter platinum disc electrode. (B) Cyclic voltammograms (scan rate 10 mVs^{-1}) obtained at rocking rates of (i) 0.83 Hz, (ii) 1.67 Hz, (iii) 8.3 Hz, (iv) 16.7, and (v) 25 Hz. (C) Plot of the mass transport limited current versus square root of rocking rate.
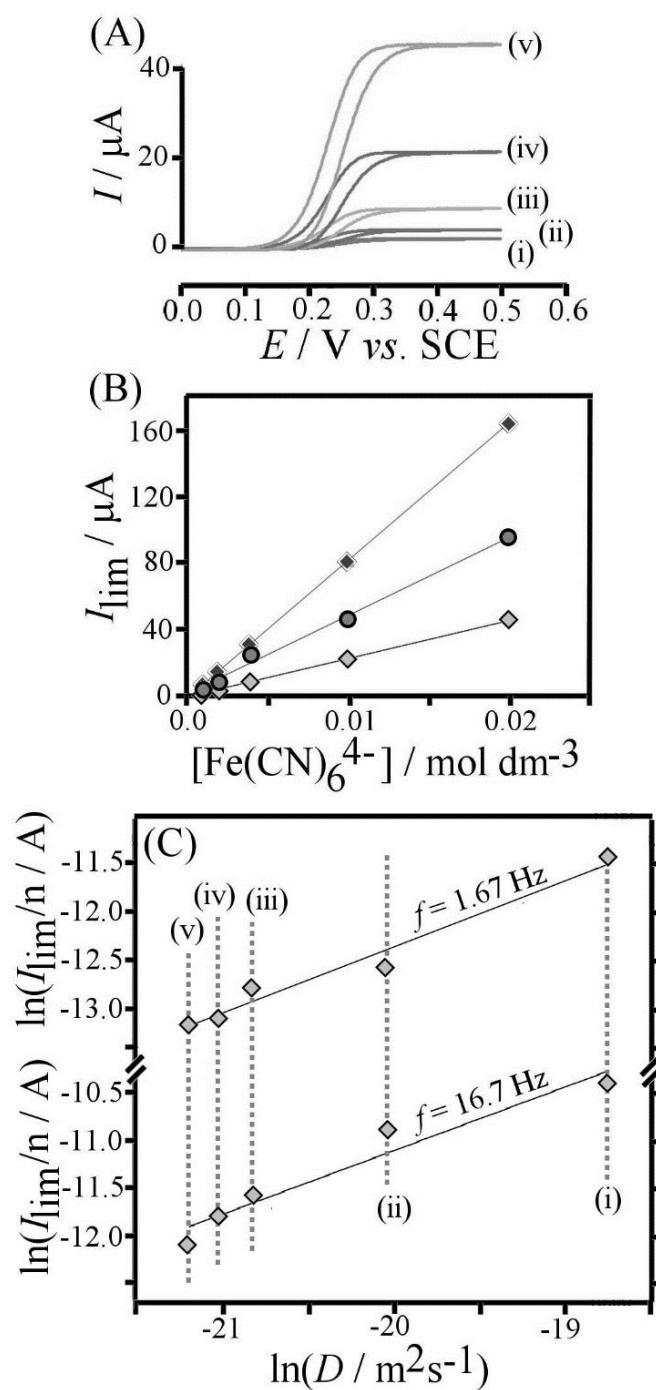
Figure 4. (A) Cyclic voltammogram (scan rate 10 mVs^{-1}) for the oxiation of (i) 1, (ii) 2, (iii) 4, (iv) 10, and (v) 20 mM Fe(CN)$_6^{4-}$ in 1 M KCl at a 1.6 mm diameter platinum electrode (rocking rate 1.67 Hz). (B) Plot of the mass transport limited current versus concentration. (C) Double-logarithmic plots of the limiting current versus diffusion coefficients (for (i) 1 mM H$^+$ reduction in 1 M KCl, (ii) 1 mM I$^-$ oxidation in 0.125 M H$_2$SO$_4$, (iii) 1 mM Ru(NH$_3$)$_6^{3+}$ reduction in 0.1 M KCl, (iv) 1 mM hydroquinone oxidation in 0.1 M phosphate buffer pH 7, and (v) 1 mM Fe(CN)$_6^{4-}$ oxidation in 1 M KCl) for f = 1.67 s^{-1} and 16.7 s^{-1}. The line of best fit in both cases shows a slope of approximately 2/3.
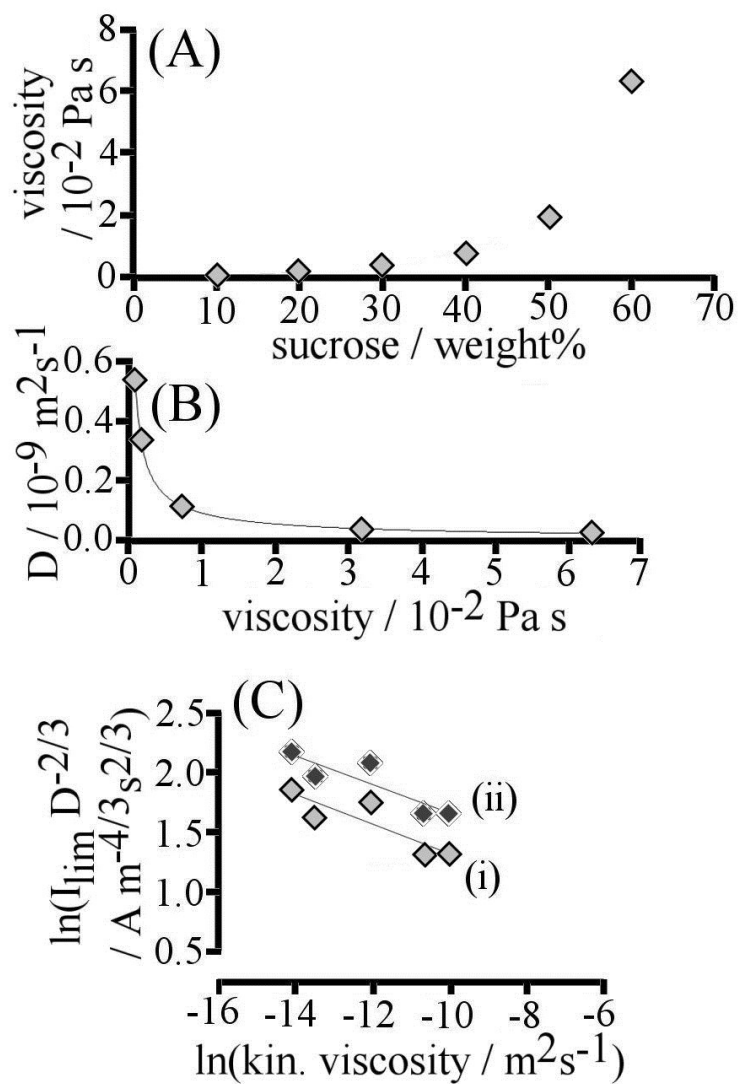
Figure 5. (A) Plot of the viscosity of water versus sucrose content in weight% [17]. (B) Plot of the diffusion coefficient of $Fe(CN)_6^{4-}$ in 1 M KCl (measured by microelectrode voltammetry) versus solution viscosity. (C) Double-logarithmic plot of the $^{D2/3}$ normalised limiting current (for 1 mM $Fe(CN)_6^{4-}$ in 1 M KCl) versus kinematic viscosity for (i) 8.3 Hz and (ii) 16.7 Hz.

Supplementary Information:
Hydrodynamic Voltammetry at a Rocking Disc Electrode: Theory *versus* Experiment

Sunyhik D. Ahn [a], Karthik Somasundaram [b], H. Viet Nguyen [b], Erik Birgersson [b],
Jim Yang Lee [b], Xiangming Gao [c], Adrian C. Fisher [c], Paul E. Frith [a], and Frank Marken*[a]

[a] *Department of Chemistry, University of Bath, Claverton Down, Bath BA2 7AY, UK*
[b] *Department of Chemical and Biomolecular Engineering, National University of Singapore, Singapore, 117576, Singapore*
[c] *Department of Chemical Engineering, University of Cambridge, New Museums Site, Pembroke Street, Cambridge, CB2 3RA, UK*

Additional Experimental Data:

Figure SI1. Cyclic voltammograms (scan rate 10 mVs^{-1}) for the reduction of 1 mM H$^+$ in 1 M KCl at a 1.6 mm diameter Pt disc electrode as a function of rocking frequency.
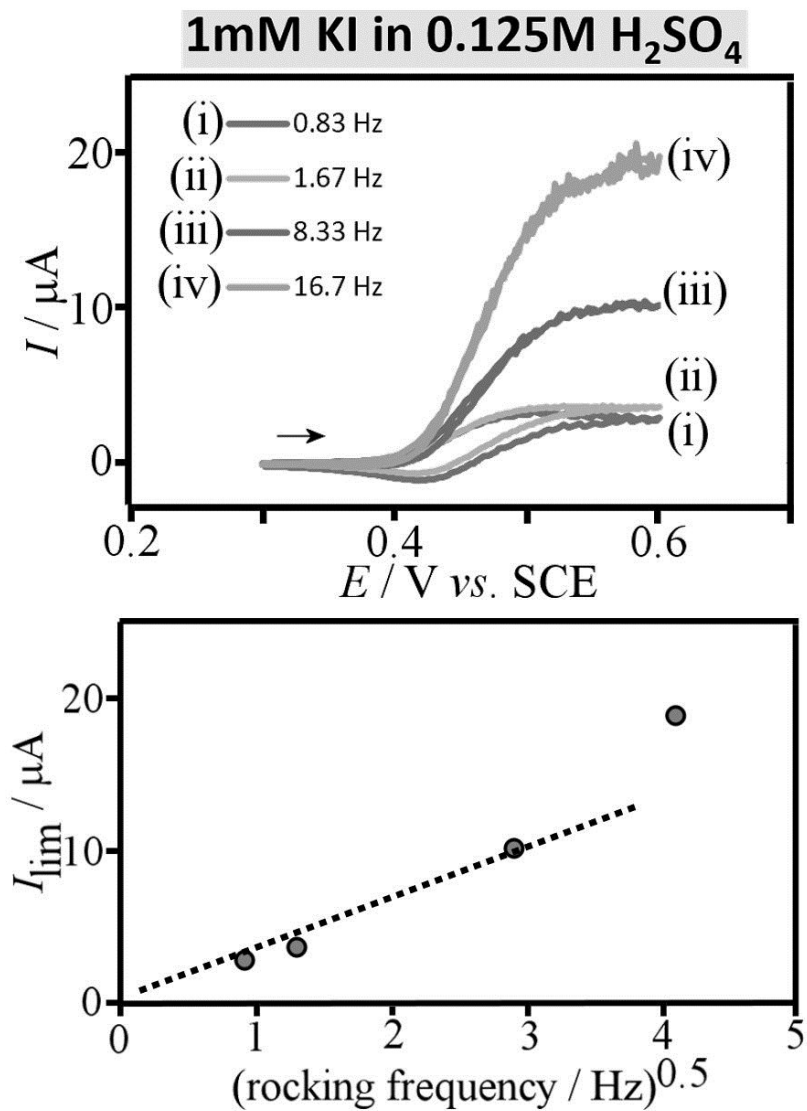
Figure SI2. Cyclic voltammograms (scan rate 10 mVs⁻¹) for the oxidation of 1 I⁻ in 0.125 M H₂SO₄ at a 1.6 mm diameter Pt disc electrode as a function of rocking frequency.
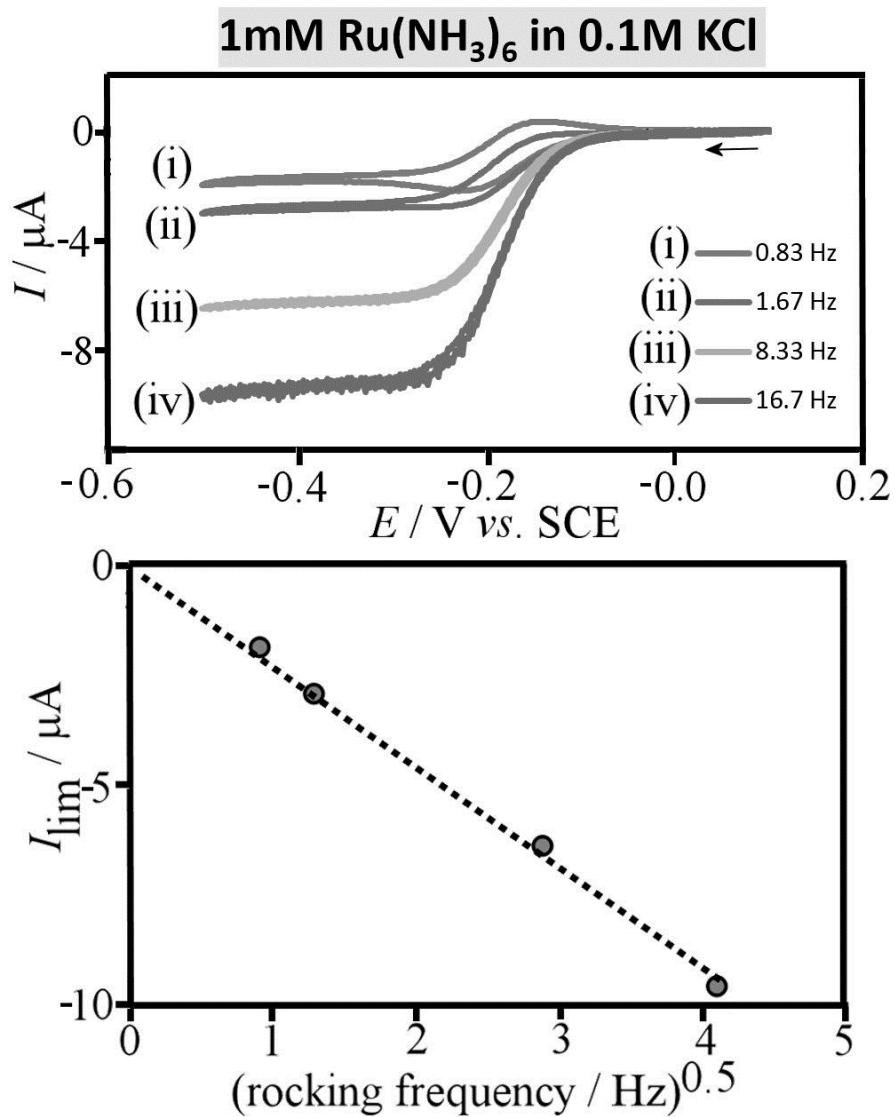
Figure SI3. Cyclic voltammograms (scan rate 10 mVs^{-1}) for the reduction of 1 mM Ru(NH$_3$)$_6$$^{3+}$ in 0.1 M KCl at a 1.6 mm diameter Pt disc electrode as a function of rocking frequency.
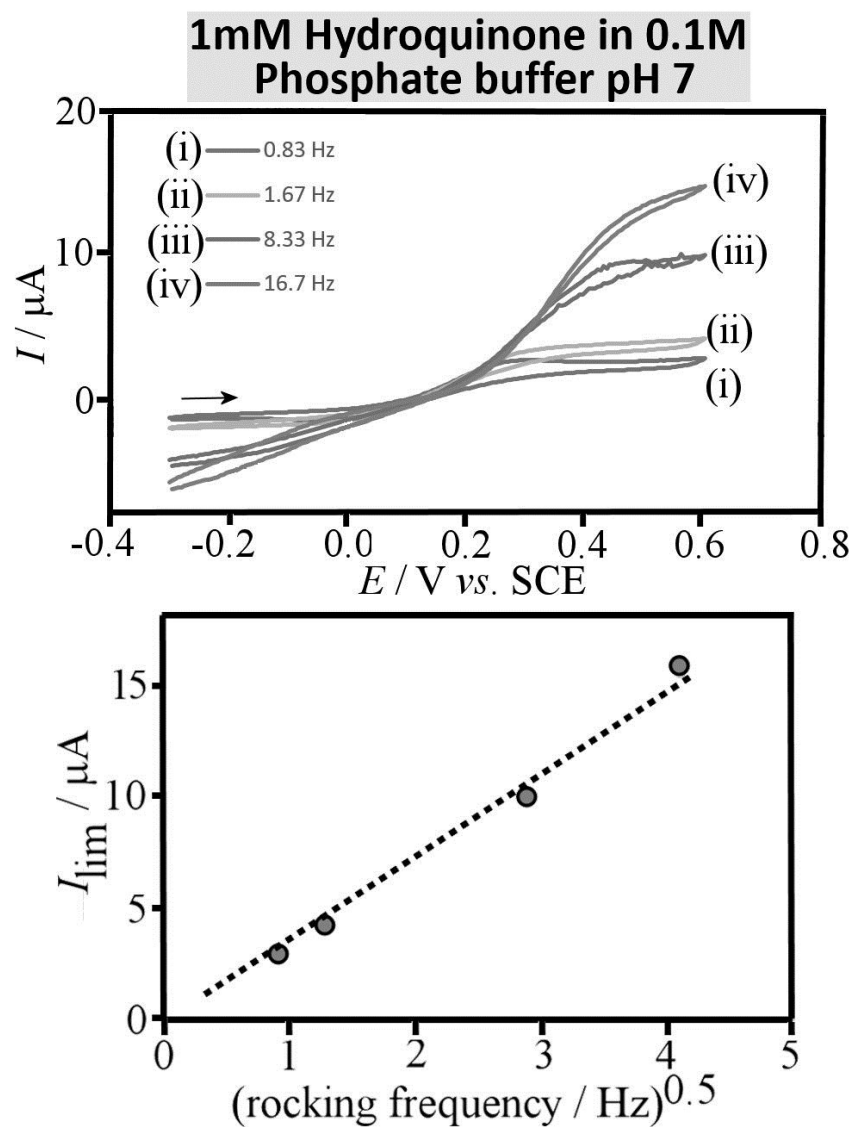
Figure SI4. Cyclic voltammograms (scan rate 10 mVs^{-1}) for the oxidation of 1 mM hydroquinone in 0.1 M phosphate buffer pH 7 at a 1.6 mm diameter Pt disc electrode as a function of rocking frequency.
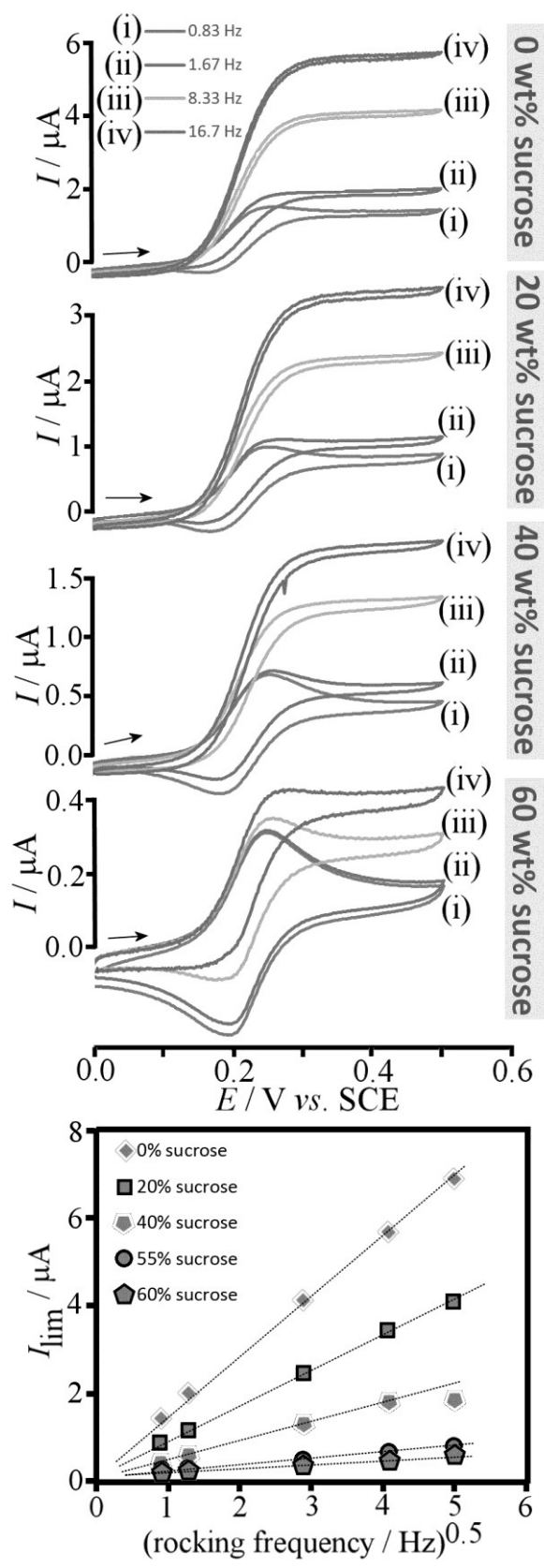
Figure SI5. Cyclic voltammograms run at 10mVs^{-1} for 1 mM Fe(CN)$_6^{4-}$ in 1 M KCl$_{(aq)}$ at various rocking frequencies with A) 0 wt% sucrose content, B) 20 wt% sucrose content, C) 40 wt% sucrose content, and D) 60 wt% sucrose content. E) The corresponding 'Levich' plot for all wt% of sucrose added.